

## Two-dimensional electron-momentum distributions for transfer ionization in fast proton-helium collisions

M. S. Schöffler,<sup>1,\*</sup> O. Chuluunbaatar,<sup>2,3</sup> S. Houamer,<sup>4</sup> A. Galstyan,<sup>5</sup> J. N. Titze,<sup>1</sup> L. Ph. H. Schmidt,<sup>1</sup> T. Jahnke,<sup>1</sup> H. Schmidt-Böcking,<sup>1</sup> R. Dörner,<sup>1</sup> Yu. V. Popov,<sup>6</sup> A. A. Gusev,<sup>2</sup> and C. Dal Cappello<sup>7</sup>

<sup>1</sup>*Institut für Kernphysik, University Frankfurt, Max-von-Laue-Strasse 1, 60438 Frankfurt, Germany*

<sup>2</sup>*Joint Institute for Nuclear Research, Dubna, Moscow Region 141980, Russia*

<sup>3</sup>*School of Mathematics and Computer Science, National University of Mongolia, Ulaanbaatar, Mongolia*

<sup>4</sup>*Département de Physique, Faculté des Sciences, Université Ferhat Abbas, Sétif 19000, Algeria*

<sup>5</sup>*Faculty of Physics, Lomonosov Moscow State University, Moscow 119991, Russia*

<sup>6</sup>*Skobel'syn Institute of Nuclear Physics, Lomonosov Moscow State University, Moscow 119991, Russia*

<sup>7</sup>*SRS MC, UMR CNRS 765, University of Lorraine, Boîte Postale 70239, F-54506 Vandoeuvre-les-Nancy, France*

(Received 6 May 2013; published 23 October 2013)

The momentum distribution of the electron in the reaction  $p + \text{He} \rightarrow \text{H} + \text{He}^{2+} + e$  is measured for projectile energies  $E_p = 300$  and  $630$  keV/u at very small scattering angles of the hydrogen. We present two-dimensional distributions parallel ( $k_{\parallel}$ ) and perpendicular ( $k_{\perp}$ ) to the projectile beam as well as distributions  $k_{\parallel}$  for fixed  $k_{\perp}$ . Theoretical calculations were carried out within the plane wave first Born approximation, which includes both mechanisms of the electron emission, namely, the shake-off and the sequential capture and ionization. It is shown that electron correlations in the initial ground-state wave function of the target play the most important role in the explanation of the experimentally observed enhanced backward electron emission.

DOI: [10.1103/PhysRevA.88.042710](https://doi.org/10.1103/PhysRevA.88.042710)

PACS number(s): 34.70.+e, 34.10.+x, 34.50.Fa

### I. INTRODUCTION

In the past decade a new wave of theoretical and experimental ion-atom collision studies on electron capture processes, involving two active electrons, such as double capture, transfer ionization (TI), and transfer excitation, has shed light on the various aspects of electron correlation. New experimental techniques allowed one to measure more than only total or single differential cross section (SDCS). Fully differential cross sections (FDCS), which depend on the momentum distribution of the escaped electron in TI, give a rather detailed view on the underlying dynamics. In this paper we consider, in particular, the reaction  $p + \text{He} \rightarrow \text{H} + \text{He}^{2+} + e^-$  at impact energies of  $E_p = 300$  and  $630$  keV. The main question we will focus on is, whether the experimental findings originate from an initial state correlation [1–4] or a dynamical correlation [5,6] between the electron during the collision or in the final state.

In TI two electrons are removed from the target; one of them is found in the continuum and the other in a bound state of the projectile. The internal dynamics is, however, versatile and strongly depends on the projectile velocity  $v_p$  and charge. Transfer ionization can proceed via two independent projectile-target interactions (sequentially) or in only one projectile-target interaction (nonsequentially). Both of these major routes have additional various pathways, especially as different mechanisms exist for the electron transfer itself. At first we will discuss the electron transfer itself, followed by a detailed description of the known combined TI processes.

An intuitive picture suggests that the electron capture is most likely to happen when the projectile and initial electron velocity vector are the same. In quantum mechanics, Oppenheimer, Brinkmann, and Kramers (OBK) showed nearly

a century ago that the electron transfer most likely happens when the electron velocity is half of the projectile velocity  $v_p$ . In their theory (OBK) the electron transfer can proceed via a momentum space overlap of the initial target and the final projectile wave function(s), which are displaced by the  $v_p$  [7]. At high projectile velocities the electron is captured from the target's high-momentum tail of the initial state wave function. As a result the capture probability scales with  $v_p^{-12}$  [8]. This is also known as kinematical capture.

At about the same time as OBK, Thomas suggested a classical mechanism for electron capture. This second-order process accelerates an electron from rest to projectile velocity [9] via a violent collision between the projectile and one target electron. This accelerated electron scatters at the target nucleus (Ne) or another electron (ee). These two consecutive binary collisions lead under special geometrical conditions to an electron propagating parallel to the projectile with the same velocity. The probability for a Thomas process scales with  $v_p^{-11}$  and is at very high energies more likely than capture by the OBK mechanism. Details can be found in [9,10] and experimental results in [11–13]. Both Thomas processes are only relevant at projectile velocities  $v_p$  much higher than those investigated here.

At even higher energies a high energetic  $\gamma$ -quant is emitted to carry away the energy from the relative motion. This process is known as radiative capture [14].

The electron emission of the transfer ionization process can either be caused by the electron capture or is initialized by an additional projectile-target interaction. The four processes of lowest order are discussed in the following paragraphs: (a) ee- and Ne-Thomas process, (b) sequential process with electron (knock-off), (c) nonsequential (shake-off), and (d) electron-electron-Auger process.

(a) While the Ne-Thomas process only transfers the electron, the electron-electron-Thomas process automatically causes a transfer ionization. In the latter case the electron,

\*schoeffler@atom.uni-frankfurt.de

which is being emitted at  $90^\circ$  with respect to the incoming projectile, is found in momentum space at  $k_{\parallel} = 0$ ,  $k_{\perp} = v_p$  (scattering plane).

(b) The sequential process, also known as two-step-2 (TS2) [15,16], usually consists in an OBK-type electron capture, followed by a second (independent) interaction of the projectile with the remaining target electron. If the momentum transfer is large enough, the electron will be knocked off, otherwise it might be just excited [17]. The experimental fingerprint of this process is a forward emission of the electron ( $k_{\parallel} > 0$ ), due to the binary character of the projectile-electron collision. In terms of the Born series and the theoretical description, TS2 first consists in a kick with a bound electron followed by capture of the remaining target electron.

(c) A sudden electron removal due to the OBK-type capture causes the wave function of the remaining electron to collapse onto the new eigenstates. With a few percent probability this leads to the emission of an electron, known as shake-off (SO) [18]. As first suggested by experimenters Mergel *et al.* [19,20] and theoretically proven by various groups [1–3,21], this correlated SO process carries a fingerprint of the initial state wave function of the target. The emission pattern, peaking in the backward direction ( $k_{\parallel} < 0$ ) is very sensitive to angular and radial electron-electron correlations [22]. In experiments performed with much better experimental resolution the direct measurement of the electron momentum vector and the selection of the final electronic state were carried out by Schöffler *et al.* [2,4,23] during the decade following the experiments by Mergel *et al.* The only fully differential calculations showing two-dimensional (2D) momentum distributions were carried out by Schöffler and co-workers [4]. They all have in common that an enhanced backward electron emission was observed, which was explained by the tiny so-called non- $s^2$  contributions in the helium ground-state wave function.

(d) The electron-electron-Auger process (eeA) was recently proposed by Voitkiv *et al.* [5] and currently challenged by Popov [24]. This process is related to the radiative capture. Instead of a photon carrying away the energy, the second electron picks up the energy being emitted backward. This results in a similar electron longitudinal momentum distribution than in (c) [6]. Popov *et al.* claim that eeA is not an independent capture mechanism, but rather a part of the OBK *post*-form [24].

The Thomas, TS2, and SO processes can easily be distinguished in the final state momentum space. The calculations of the eeA process published so far are of low differentiability. Calculations being differential in the projectile scattering plane or differential in the scattering angle are unfortunately not available at present. Comparison of calculations for the eeA with experimental data so far was restricted to single differential cross sections, showing the electron longitudinal momentum distribution [6]. The calculated longitudinal momenta from eeA and shake-off are, however, rather similar for the collision systems studied so far. We will provide here data which show the two-dimensional momentum distributions in the longitudinal vs transversal representation. We compare the experimental results with calculated FDCS within the plane wave first Born approximation (PWFBA) on proton-helium interaction at impact energies of 300 and 630 keV. Both of the above discussed mechanisms, SO and TS2, contribute in this case. We have

to note that PWFBA fully corresponds to the first Coulomb-Born approximation (CB1-model) [16]. Atomic units  $\hbar = e = m_e = 1$  are used throughout unless otherwise specified.

## II. EXPERIMENT

To achieve the goals of this experiment all emitted particles have to be measured in coincidence. Therefore we applied momentum spectroscopy techniques, such as reaction microscopes or COLTRIMS (cold target recoil ion momentum spectroscopy) [25–27]. The experiments were performed at the Institut für Kernphysik at the University of Frankfurt using the Van de Graaff accelerator. Using three sets of movable slits, the proton beam was collimated to a divergence  $\leq 0.15$  mrad, a size of about  $0.5 \times 0.5$  mm<sup>2</sup> at the overlap region with the gas jet. 15 cm upstream of the target, a set of parallel electrostatic deflector plates cleaned the primary beam from charge state impurities, deflecting the primary beam slightly upwards. The proton beam was crossed perpendicular with the helium gas jet. 15 cm downstream from the target a second set of horizontal electrostatic deflector plates separate the final charge state, thus only the neutral projectiles H hit a position and time sensitive microchannel plate (MCP) detector, placed 3 m downstream from the interaction point, yielding the projectile deflection angle and the time zero of the collision. The main part of the beam ( $\approx 1$  nA), which is still charged was dumped in a Faraday cup.

The gas jet providing the target beam was generated by helium gas expanding through a 30- $\mu$ m nozzle with a backing pressure of 20 bars and collimated in a two stage jet. A density of  $5 \times 10^{11}$  atoms/cm<sup>2</sup> and a diameter of 1.5 mm were achieved. The active cooling by the supersonic expansion combined with the passive one in the perpendicular direction by the geometry resulted in a three-dimensional cold target and a momentum uncertainty below 0.1 atomic units (a.u.).

At the overlapping volume where the proton and helium beams were intersected, electrons and ions were created. A weak electrostatic field of 4.8 V/cm was applied to project electrons and recoiling ions onto two position and timesensitive detectors. To optimize the resolution, a three-dimensional time and space focusing geometry [28,29] was used for the recoil ion arm of the spectrometer. The ions were detected by an 80-mm-diameter microchannel plate detector with delay-line anode [30,31]. The time focusing was realized using a field-free drift tube [32], while an adjustable electrostatic lens was used to achieve space focusing. This lens was optimized by minimizing the spatial width of the lines on the detector from He<sup>+</sup> ions created by pure capture, which have been recorded parallel to the transfer ionization events (for an example, see Fig. 1 in [33] or Fig. 1 in [34]). A momentum resolution of 0.1 a.u. was achieved in all three directions. The electrons were guided by a magnetic field (see [35]) of 15 and 25 Gauss and accelerated over a length of 20 cm by the same electric field in a time focusing geometry (40 cm additional field-free drift tube) onto a MCP detector of 120 mm active diameter. The overall spectrometer geometry, especially the ion's part was simulated using SIMION to gain the maximum resolution and efficiency.

We reached an overall acceptance of  $4\pi$  solid angle for recoil ions up to a momentum of 10 a.u. and electrons up to 6 a.u. A three-particle coincidence (H + He<sup>2+</sup> + e<sup>-</sup>) was

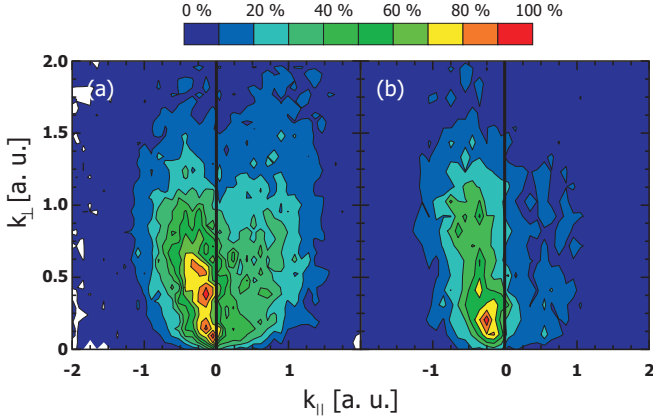


FIG. 1. (Color online) Experimental momentum distribution of the electron for (a)  $E_p = 300$  keV and (b)  $E_p = 630$  keV. The projectile is moving in the positive  $k_{\parallel}$  direction, i.e., from the left to the right. The data are integrated over all other observables, i.e., the integral over the shown distribution corresponds to the total transfer ionization cross section for the  $H(n = 1)$  state.

applied to record the data event by event. From the positions of impact on the detectors and the time of flight we can derive the momentum vectors of the recoil ion and the electron. The projectile transverse momentum vectors were directly measured. Checking energy and momentum conservation the background was strongly suppressed during the off-line data analysis. Also the overall resolution was good enough to measure the final electronic state of the H and separate events where the hydrogen was found in the ground state from where the electron was captured into an excited state. Only these events, where the hydrogen is in the ground state are presented in the following.

### III. THEORY

As stated above, we consider the He atom as a target for the TI reaction. We follow definitions and notations given in [36] and do not repeat all conditions here. In the momentum representation in the laboratory frame and at very small scattering angle  $\theta_p$  the nonsymmetrized matrix element is given in its *prior*-form by

$$\begin{aligned} \mathcal{T}_{\text{FBA}} = & 4\pi\sqrt{2} \int \frac{d\vec{x}}{(2\pi)^3} \frac{\tilde{\phi}_H(x)}{|\vec{v}_p - \vec{q} - \vec{x}|^2} [Z_p Z_e F(\vec{q}; 0; \vec{k}) \\ & + Z_p Z_e F(\vec{v}_p - \vec{x}; \vec{v}_p + \vec{q} + \vec{x}; \vec{k}) \\ & + Z_p Z_N F(\vec{v}_p - \vec{x}; 0; \vec{k})] = A1 + A2 + A3, \\ Z_p = & +1, \quad Z_N = +2, \quad Z_e = -1, \end{aligned} \quad (1)$$

where

$$F(\vec{y}; \vec{\eta}; \vec{k}) = \int e^{-i\vec{y}\vec{r}_1 - i\vec{\eta}\vec{r}_2} \phi_c^{-*}(\vec{k}, \vec{r}_2) \Phi_0(\vec{r}_1, \vec{r}_2) d\vec{r}_1 d\vec{r}_2, \quad (2)$$

$\vec{v}_p$  is the fast proton velocity,  $\vec{q}$  is the transferred momentum ( $\vec{q} = \vec{p}_H - \vec{p}_p$ ),  $\vec{k}$  is the electron momentum, and  $\Phi_0(\vec{r}_1, \vec{r}_2)$  is the the helium ground wave function. The ejected electron is described by a Coulomb wave function of the final target ion

$$\begin{aligned} \phi_c^{-*}(\vec{k}, \vec{r}) = & e^{-\pi\xi/2} \Gamma(1 + i\xi) e^{-i\vec{k}\vec{r}} {}_1F_1(-i\xi, 1; i\vec{k}\vec{r} + i\vec{k}\vec{r}); \\ \xi = & Z_e Z_N / v_{Ne}. \end{aligned}$$

The FDCS is calculated by the formula

$$\frac{d^2\sigma}{dk_{\perp} dk_{\parallel}} = \frac{m_p^2 k_{\perp}}{(2\pi)^4} \int_0^{\theta_{\max}} \theta_p d\theta_p \int_0^{2\pi} d\phi_k |A1 + A2 + A3|^2, \quad (3)$$

with  $m_p = 1836.15$  being the proton mass. We display all vectors' components for clarity:  $\vec{v}_p = \{0, 0, v_p\}$ ,  $\vec{q} = \{m_p v_p \theta_p, 0, q_{\parallel}\}$ , and  $\vec{k} = \{k_{\perp} \cos \phi_k, k_{\perp} \sin \phi_k, k_{\parallel}\}$ . We also remind one that  $q_{\parallel} = v_p/2 + Q/v_p$  with  $Q = E_0^{\text{He}} - E^{\text{H}} - k^2/(2m_e)$ .

These approximate relations are obtained from the energy and momentum conservation, whose corresponding exact expressions are

$$q_{\parallel} = \mu_{ep} v_p / 2 + Q / v_p,$$

$$Q = E_0^{\text{He}} - E^{\text{H}} - k^2 / (2m_e) - K_N^2 / (2m_N) - q^2 / (2m_H)$$

and

$$\vec{K}_N = -\vec{q} - \vec{k}. \quad (4)$$

For very small scattering angles  $\theta_p$ , when  $q$  does not exceed 10 a.u., and the electron energy is also a few atomic units, both the energy of nucleus  $K_N^2/(2m_N)$  and the value  $q^2/(2m_H)$  are very small due to huge masses of the nucleus  $m_N$  and hydrogen  $m_H$ . This means that the nucleus stays practically immovable during the collision time. Also the reduced mass

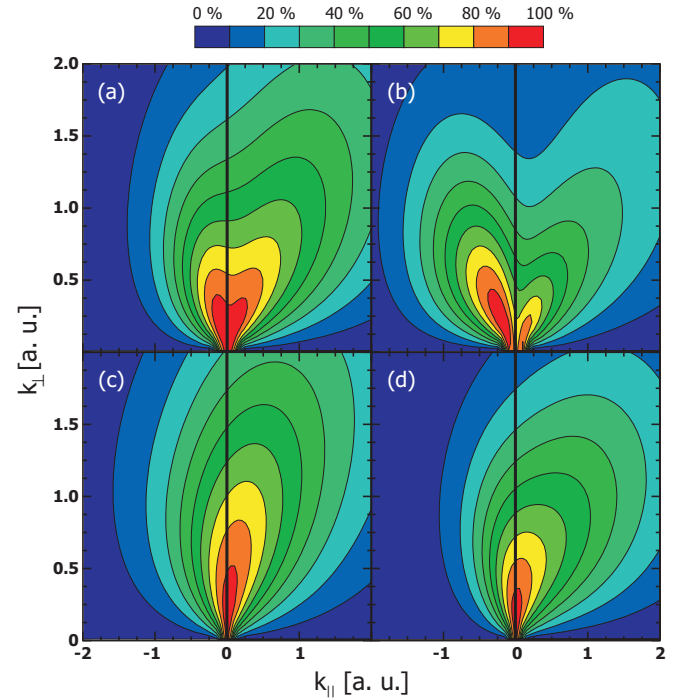


FIG. 2. (Color online) Electron momentum distribution as a function of the longitudinal and transversal momentum component, calculated within the PWFBA for (a)  $E_p = 300$  keV using a highly correlated initial state wave function, (b)  $E_p = 630$  keV also using a highly correlated initial state wave function, (c)  $E_p = 300$  keV using a weakly correlated initial state wave function RHF [37], and (d)  $E_p = 630$  keV using the same weakly correlated initial state wave function RHF [37]. In (a) and (b) both highly correlated wave functions [38] and [39] give practically indistinguishable distributions.

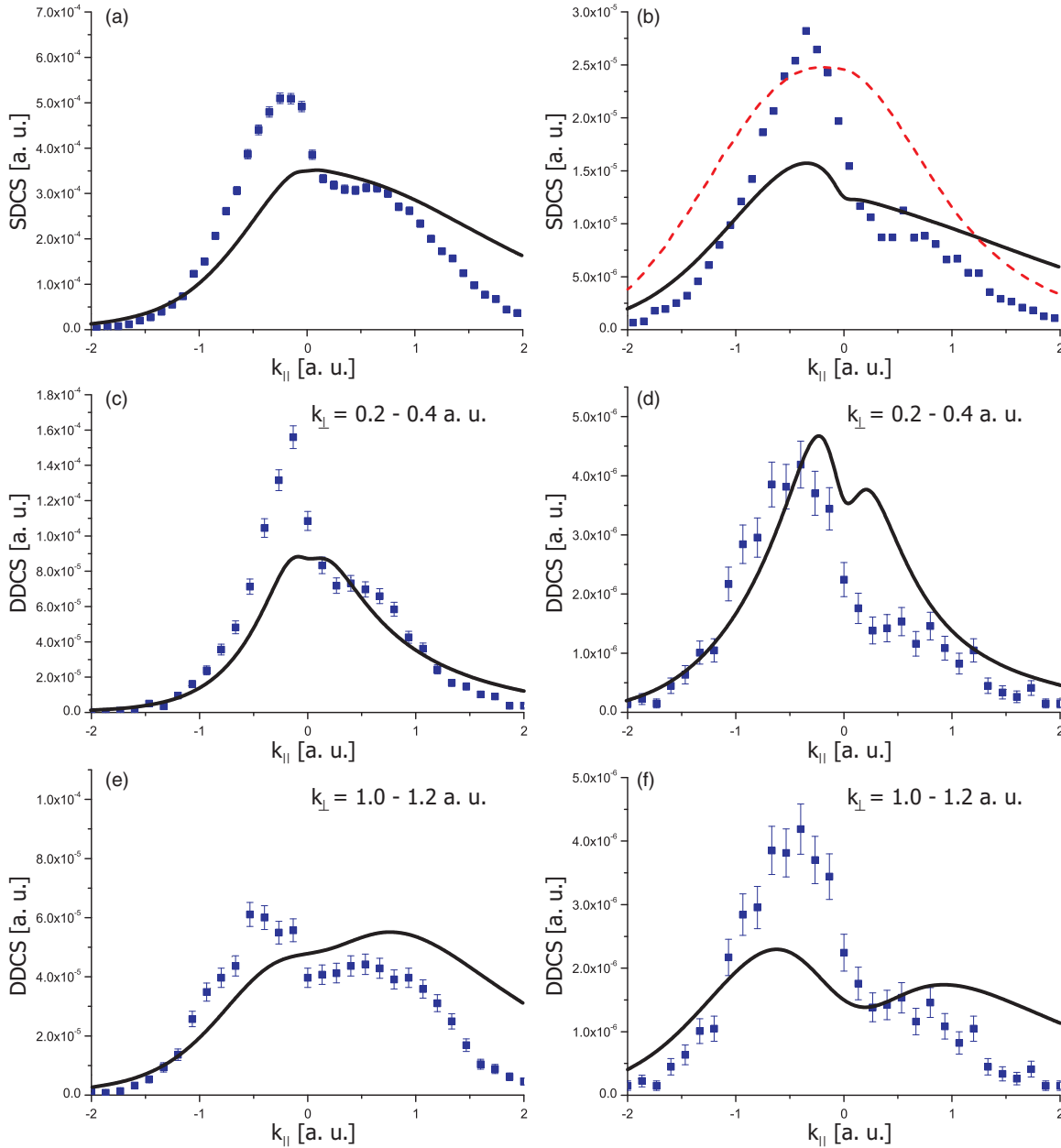


FIG. 3. (Color online) Electron longitudinal momentum ( $k_{||}$ ) at  $E_p = 300$  keV (left column) and  $E_p = 630$  (right column). Solid line: PWFBA using the highly correlated wave function [38]. Dots are experimental points of the present work. (a) and (b) show the SDCS, e.g., integrated over all  $k_{\perp}$ . The (red) dashed line in (b) is a result of calculations based on the eeA mechanism; it was taken from Fig. 2(a) in [6]; (c) and (d) display DDCS for fixed  $k_{\perp} = 0.2\text{--}0.4$  a.u.; (e) and (f) same but for  $k_{\perp} = 1.0\text{--}1.2$  a.u. The experimental data were normalized to published values [42].

$\mu_{ep} \approx m_e = 1$ . As well, the relative velocity of the immovable nucleus and ionized electron  $v_{Ne} \approx k$ .

In (1) the term  $A_1$  is the OBK amplitude, where any trial helium wave function can be used. The amplitude  $A_3$  can be attributed to SO. It describes the contribution of heavy particles interaction. The amplitude  $A_2$  is a typical PWFBA realization of the TS2 mechanism (ionization via electron knock-off).

#### IV. RESULTS AND DISCUSSION

For calculations we use three trial helium wave functions. One is the loosely correlated  $1s^2$  Roothan-Hartree-Fock (RHF)

function of Clementi and Roetti [37] ( $E_0^{\text{He}} = -2.8617$ ). The two others are highly correlated functions. One of them is a type

$$\Psi(r_1, r_2, r_{12}) = \sum_{j=1}^N D_j [\exp(-\alpha_j r_1 - \beta_j r_2) + \exp(-\alpha_j r_2 - \beta_j r_1)] \exp(-\gamma_j r_{12}), \quad (5)$$

which was described in [38] ( $E_0^{\text{He}} = -2.9037$ ). The other highly correlated function is the configuration interaction wave function proposed by Mitroy *et al.* [39] ( $E_0^{\text{He}} = -2.9031$ ).

The experimental data at  $E_p = 300$  and  $E_p = 630$  keV, shown in Fig. 1, display a noticeable peak at the backward (negative  $k_{\parallel}$ ) direction and a less resolved peak at the forward direction (positive  $k_{\parallel}$ ). The forward peak structure is more intense at the lower projectile energy of 300 keV, as the projectile-target interaction time is longer and therefore an additional interaction, the electron knock-off, is more likely to occur.

As expected, calculations with the loosely correlated wave function [Figs. 2(c) and 2(d)] give practically no backward peak to the electron's distribution. The highly correlated helium wave function gives very similar distributions [Figs. 2(a) and 2(b)], which include both forward and backward peaks. However, visually they are hard to compare with the experiment.

To avoid effects of color scales and for comparison with other published theoretical results, we present for 300 and 630 keV the longitudinal electron momentum distribution ( $k_{\parallel}$ ) in Figs. 3(a) and 3(b). Additionally two slices of the distributions from Figs. 1 and 2 for fixed  $k_{\perp}$  are shown:  $k_{\perp} = 0.2\text{--}0.4$  a.u. in Figs. 3(c) and 3(d) and  $k_{\perp} = 1.0\text{--}1.2$  a.u. in Figs. 3(e) and 3(f). The experimental data points have been normalized to published values [42]. Figure 3(b) also contains the calculation from [6], based on the eeA process. In particular, at 630 keV/u, our theory reproduces the main features as the splitting into a forward and a backward peak, nicely. In contrast the (red) dashed curve from [6] represents an incoherent sum of the eeA, TS2, and SO. Its shape is structureless and has a 50% larger total cross section compared to the experiment and our calculations (see also [24] for a critical discussion of the eeA process). A proper calculation with a coherent sum of these processes might result in a better agreement. The nice agreement of our theory and experiment for  $k_{\parallel} < 0$  demonstrates that the PWFBA shake-off amplitude is quite sufficient to describe the backward peak. This requires of course, the use of highly correlated target wave functions. At larger projectile scattering angles, the theory underestimates the experimental data in the backward direction, but noticeably exceeds the experimental points in the forward domain  $k_{\parallel} > 0$ . It is a clear indication that second-order Born calculations are needed here. Unfortunately, we cannot provide these calculations at the moment.

To substantiate the generality of the SO behavior, we present in Fig. 4 the momentum of the backward emitted electron as a function of the projectile velocity for various projectiles ( $p$ ,  $\text{He}^+$ , and  $\text{He}^{2+}$ ). Independent of the projectile, whether it is singly ( $p$ ) or doubly ( $\text{He}^{2+}$ ) charged, its potential is screened (as for  $\text{He}^+$ ) or not, the peak momentum is always the same and increases with the projectile velocity. A similar result was already found for proton impact by Mergel *et al.* [19] and theoretically described in [21]. This finding supports the idea of SO and that the electron distribution only depends on the nature of the target, while the eeA process is sensitive to both the target and the projectile.

We finally show a comparison of the total transfer ionization cross section obtained in the PWFBA theory, using the helium wave function proposed by Mitroy *et al.* [39], and experiment. In Fig. 5 the agreement is quite satisfactory over a wide range of the proton energies (see also [40]).

From these findings, which can be explained within the PWFBA and from what has been published for the eeA, one

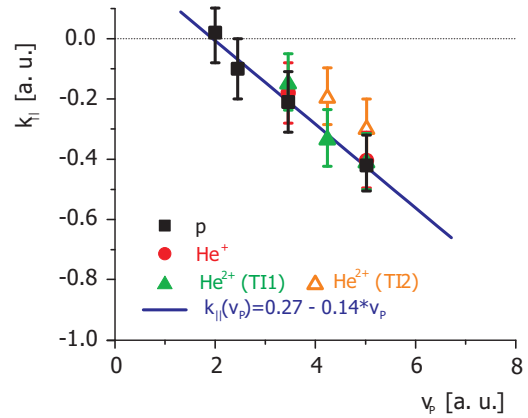


FIG. 4. (Color online) Peak position of the backward emitted electrons as a function of the projectile velocity for protons (black squares),  $\text{He}^+$  (red circles), and  $\text{He}^{2+}$  projectiles (triangles). The  $\text{He}^{2+}$  projectiles data are divided into the final electronic state, whether the captured electron is in the  $\text{He}^+$  ground state (green solid triangle) or in an excited state (open orange triangles). A linear fit through these data points to guide the eye is shown as a solid line.

may conclude that both explanations match the experimental observations. The good agreement in the fully differential cross sections favors SO and non- $s^2$  states being the correct explanation for backward emitted electrons. The eeA so far has only shown a good agreement in single differential cross sections; the detailed comparison in FDCS stays open. Furthermore, if both theoretical descriptions resulted in the same momentum distribution, following Occam's razor, we would clearly prefer PWFBA, the "simpler" process, as explanation.

## V. CONCLUSIONS

In conclusion, we presented highly differential theoretical (PWFBA) results and measured data from a kinematically complete experiment on transfer ionization in proton on helium

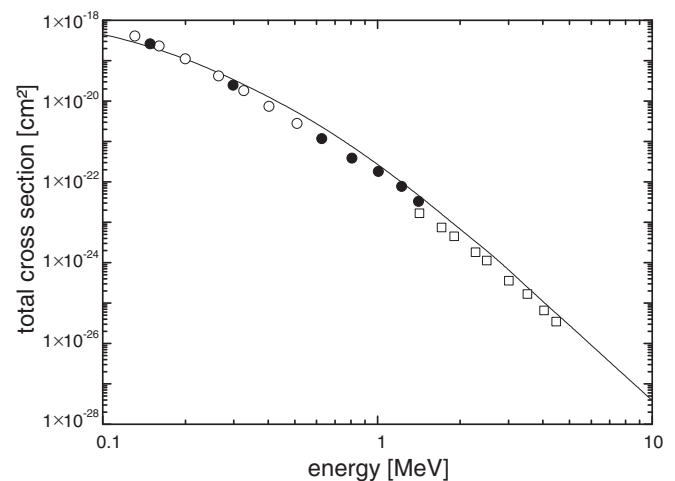


FIG. 5. Total cross section for transfer ionization for different proton energies  $E_p$  (solid line), using the wave function proposed by Mitroy *et al.* [39]. Experiment: open circles, Shah and Gilbody [41]; full circles, Mergel *et al.* [42]; open squares, Schmidt *et al.* [43].

collision at 300 and 630 keV. The observed splitting into forward and backward emission originates from two different contributions, the  $A_2$  term (binary encounter) and the  $A_1 + A_3$  term (shake-off). Comparison of loosely and highly correlated wave functions for the initial state confirms the high sensitivity of the experiment to the subtle features of the initial state wave function. Better agreement for the forward emitted electrons can be expected from calculations carried out in second order. At the same time, backward emitted electrons can be described within the first Born approximation at high projectile energies.

## ACKNOWLEDGMENTS

We acknowledge financial support from the Deutsche Forschungsgemeinschaft (DFG), Grant No. SCHO 1210/2-1. As well, this work was partially supported by Russian Foundation of Basic Research (RFBR), Grant No. 11-01-00523-a. All calculations were performed using Moscow State University Research Computing Centre (supercomputers Lomonosov and Chebyshev) and Joint Institute for Nuclear Research Central Information and Computer Complex. The authors are grateful to K. A. Kouzakov for inspiring discussions and help.

- 
- [1] A. Godunov, C. T. Whelan, and H. R. J. Walters, *J. Phys. B: At., Mol. Opt. Phys.* **37**, L201 (2004).
- [2] M. Schöffler, A. L. Godunov, C. T. Whelan, H. R. J. Walters, V. S. Schipakov, V. Mergel, R. Dörner, O. Jagutzki, L. Ph. H. Schmidt, J. Titze, E. Weigold, and H. Schmidt-Böcking, *J. Phys. B: At., Mol. Opt. Phys.* **38**, L123 (2005).
- [3] A. L. Godunov, C. T. Whelan, H. R. J. Walters, V. S. Schipakov, M. Schöffler, V. Mergel, R. Dörner, O. Jagutzki, L. Ph. H. Schmidt, J. Titze, and H. Schmidt-Böcking, *Phys. Rev. A* **71**, 052712 (2005).
- [4] M. S. Schöffler, O. Chuluunbaatar, Yu. V. Popov, S. Houamer, J. Titze, T. Jahnke, L. Ph. H. Schmidt, O. Jagutzki, A. G. Galstyan, and A. A. Gusev, *Phys. Rev. A* **87**, 032715 (2013).
- [5] A. B. Voitkiv, B. Najjari, and J. Ullrich, *Phys. Rev. Lett.* **101**, 223201 (2008).
- [6] M. Schulz, X. Wang, M. Gundmundsson, K. Schneider, A. Kelkar, A. B. Voitkiv, B. Najjari, M. Schöffler, L. Ph. H. Schmidt, R. Dörner, J. Ullrich, R. Moshhammer, and D. Fischer, *Phys. Rev. Lett.* **108**, 043202 (2012).
- [7] J. R. Oppenheimer, *Phys. Rev.* **31**, 349 (1928); H. C. Brinkman and H. A. Kramers, *Proc. R. Acad. Sci. Amsterdam* **33**, 973 (1930).
- [8] D. Belkic and A. Salin, *J. Phys. B: At. Mol. Phys.* **11**, 3905 (1978).
- [9] L. H. Thomas, *Proc. R. Soc. London, Ser. A* **114**, 561 (1927).
- [10] J. S. Briggs and K. Taulbjerg, *J. Phys. B: At. Mol. Phys.* **12**, 2565 (1979).
- [11] E. Horsdal-Pedersen, C. L. Cocke, and M. Stockli, *Phys. Rev. Lett.* **50**, 1910 (1983).
- [12] D. Fischer, K. Stochkel, H. Cederquist, H. Zettergren, P. Reinhard, R. Schuch, A. Kallberg, A. Simonsson, and H. T. Schmidt, *Phys. Rev. A* **73**, 052713 (2006).
- [13] J. Palinkas, R. Schuch, H. Cederquist, and O. Gustafsson, *Phys. Rev. Lett.* **63**, 2464 (1989).
- [14] J. Eichler and T. Stöhlker, *Phys. Rep.* **439**, 1 (2007).
- [15] R. Shakeshaft and L. Spruch, *Rev. Mod. Phys.* **51**, 369 (1979).
- [16] D. Belkic, I. Mancev, and J. Hanssen, *Rev. Mod. Phys.* **80**, 249 (2008).
- [17] M. S. Schöffler, J. N. Titze, L. Ph. H. Schmidt, T. Jahnke, O. Jagutzki, H. Schmidt-Böcking, and R. Dörner, *Phys. Rev. A* **80**, 042702 (2009).
- [18] T. Åberg, *Phys. Rev.* **156**, 35 (1967).
- [19] V. Mergel, R. Dörner, K. Khayyat, M. Achler, T. Weber, O. Jagutzki, H. J. Lüdde, C. L. Cocke, and H. Schmidt-Böcking, *Phys. Rev. Lett.* **86**, 2257 (2001).
- [20] H. Schmidt-Böcking, V. Mergel, R. Dörner, C. L. Cocke, O. Jagutzki, L. Schmidt, Th. Weber, H. J. Lüdde, E. Weigold, J. Berakdar, H. Cederquist, H. T. Schmidt, R. Schuch, and A. S. Kheifets, *Europhys. Lett.* **62**, 477 (2003).
- [21] T. Y. Shi and C. D. Lin, *Phys. Rev. Lett.* **89**, 163202 (2002).
- [22] N. Watanabe, Y. Khajuria, M. Takahashi, Y. Udagawa, P. S. Vinitsky, Yu. V. Popov, O. Chuluunbaatar, and K. A. Kouzakov, *Phys. Rev. A* **72**, 032705 (2005).
- [23] M. S. Schöffler, Ph.D. thesis, Johann Wolfgang Goethe-Universität, Frankfurt am Main, 2006.
- [24] Yu. V. Popov, V. L. Shablov, K. A. Kouzakov, and A. G. Galstyan, arXiv:1304.3045v2.
- [25] J. Ullrich, R. Moshhammer, R. Dörner, O. Jagutzki, V. Mergel, H. Schmidt-Böcking, and L. Spielberger, *J. Phys. B: At., Mol. Opt. Phys.* **30**, 2917 (1997).
- [26] R. Dörner, V. Mergel, O. Jagutzki, L. Spielberger, J. Ullrich, R. Moshhammer, and H. Schmidt-Böcking, *Phys. Rep.* **330**, 95 (2000).
- [27] J. Ullrich, R. Moshhammer, A. Dorn, R. Dörner, L. Ph. H. Schmidt, and H. Schmidt-Böcking, *Rep. Prog. Phys.* **66**, 1463 (2003).
- [28] M. S. Schöffler, T. Jahnke, J. Titze, N. Petridis, K. Cole, L. Ph. H. Schmidt, A. Czasch, O. Jagutzki, J. B. Williams, C. C. Cocke, T. Osipov, S. Lee, M. H. Prior, A. Belkacem, A. L. Landers, H. Schmidt-Böcking, R. Dörner, and Th. Weber, *New J. Phys.* **13**, 095013 (2011).
- [29] V. Mergel, R. Dörner, J. Ullrich, O. Jagutzki, S. Lencinas, S. Nüttgens, L. Spielberger, M. Unverzagt, C. L. Cocke, R. E. Olson, M. Schulz, U. Buck, E. Zanger, W. Theisinger, M. Isser, S. Geis, and H. Schmidt-Böcking, *Phys. Rev. Lett.* **74**, 2200 (1995).
- [30] O. Jagutzki, J. S. Lapington, L. B. C. Worth, U. Spillman, V. Mergel, and H. Schmidt-Böcking, *Nucl. Instrum. Methods Phys. Res., Sect. A* **477**, 256 (2002).
- [31] O. Jagutzki, V. Mergel, K. Ullmann-Pfleger, L. Spielberger, U. Spillmann, R. Dörner, and H. Schmidt-Böcking, *Nucl. Instrum. Methods Phys. Res., Sect. A* **477**, 244 (2002).
- [32] W. C. Wiley and I. H. McLaren, *Rev. Sci. Instrum.* **26**, 1150 (1955).
- [33] M. S. Schöffler, J. Titze, L. Ph. H. Schmidt, T. Jahnke, N. Neumann, O. Jagutzki, H. Schmidt-Böcking, R. Dörner, and I. Mancev, *Phys. Rev. A* **79**, 064701 (2009).
- [34] Hong-Keun Kim, M. S. Schöffler, S. Houamer, O. Chuluunbaatar, J. N. Titze, L. Ph. H. Schmidt, T. Jahnke,

- H. Schmidt-Böcking, A. Galstyan, Yu. V. Popov, and R. Dörner, *Phys. Rev. A* **85**, 022707 (2012).
- [35] R. Moshhammer, M. Unverzagt, W. Schmitt, J. Ullrich, and H. Schmidt-Böcking, *Nucl. Instrum. Methods Phys. Res., Sect. B* **108**, 425 (1996).
- [36] S. Houamer, Yu. V. Popov, and C. Dal Cappello, *Phys. Rev. A* **81**, 032703 (2010).
- [37] E. Clementi and C. Roetti, *At. Data Nucl. Data Tables* **14**, 177 (1974).
- [38] O. Chuluunbaatar, I. V. Puzynin, P. S. Vinitzky, Yu. V. Popov, K. A. Kouzakov, and C. Dal Cappello, *Phys. Rev. A* **74**, 014703 (2006).
- [39] J. Mitroy, I. E. McCarthy, and E. Weigold, *J. Phys. B: At., Mol. Opt. Phys.* **18**, 4149 (1985).
- [40] A. L. Godunov, J. H. McGuire, V. S. Schipakov, H. R. J. Walters, and C. T. Whelan, *J. Phys. B: At. Mol. Phys.* **39**, 987 (2006).
- [41] M. B. Shah and H. B. Gilbody, *J. Phys. B: At. Mol. Phys.* **18**, 899 (1985).
- [42] V. Mergel, R. Dörner, M. Achler, Kh. Khayyat, S. Lencinas, J. Euler, O. Jagutzki, S. Nüttgens, M. Unverzagt, L. Spielberger, W. Wu, R. Ali, J. Ullrich, H. Cederquist, A. Salin, C. J. Wood, R. E. Olson, Dž. Belkić, C. L. Cocke, and H. Schmidt-Böcking, *Phys. Rev. Lett.* **79**, 387 (1997).
- [43] H. T. Schmidt, J. Jensen, P. Reinhard, R. Schuch, K. Støchkel, H. Zettergren, H. Cederquist, L. Bagge, H. Danared, A. Källberg, H. Schmidt-Böcking, and C. L. Cocke, *Phys. Rev. A* **72**, 012713 (2005).